COMPDYN 2015
5th ECCOMAS Thematic Conference on
Computational Methods in Structural Dynamics and Earthquake Engineering
M. Papadrakakis, V. Papadopoulos, V. Plevris (eds.)
Crete Island, Greece, 25–27 May 2015

EXAMINING THE INITIATION MECHANISMS OF STATIC AND DYNAMIC LIQUEFACTION USING THREE DIMENSIONAL DEM SIMULATIONS

Zitao Zhang[1] **and Yu-Hsing Wang**[2]

[1] Department of Civil and Environmental Engineering, The Hong Kong University of Science and Technology, HKSAR, China
e-mail: zzhangaf@ust.hk

[2] Department of Civil and Environmental Engineering, The Hong Kong University of Science and Technology, HKSAR, China
ceyhwang@ust.hk

Keywords: Static Liquefaction, Cyclic Loading, Contact Force Distribution, Discrete Element Method.

Abstract. *Static and dynamic liquefaction may produce different levels of damages on the infrastructures and various numbers of casualties. Understanding the associated initiation mechanisms therefore is very important for geotechnical engineers to predict and manage the relevant hazards. In this study, a series of DEM simulations of undrained triaxial compression tests and a cyclic undrained triaxial test are carried out to examine the initiation mechanisms from a micromechanical perspective. The simulation results demonstrate a continuous decrease in the mean of contact normal forces and a continuous increase in the associated COV as the shear strain increases during undrained compression of a loose sample. Such kind of evolution trend found in the contact force distribution was not observed in the simulations of undrained compression tests on medium dense to dense sand samples. However, the same behavior can be detected in the cyclic undrained triaxial tests on a dense sample, i.e., a continuous decrease in the mean of contact normal forces and a continuous increase in the associated COV. Hence, such an evolution tendency of contact force distributions can serve as a basis to explain the initiation mechanisms of the static and dynamic liquefaction from a micromechanical point of view.*

1 INTRODUCTION

Liquefaction describes a condition where the effective stress of the soil reaches a very low value (i.e., close to zero) due to the buildup of pore pressures. Liquefaction may be induced by monotonic or static loading, which is commonly referred to as static liquefaction. Static liquefaction may lead to different types of hazards, e.g., failures of the submarine slopes, dams and tailings structures, and most of these case histories occurred in very loose to loose saturated sand [1]. Even though static liquefaction can hardly occur in medium dense to dese sand, a cyclic loading, e.g., earthquake shaking, may induce the decrease in the effectives stress, and the liquefaction state might be reached after a certain number of loading cycles. Once the liquefaction state is reached, large strains might be developed in the subsequent loading cycles to cause casualties [2]. For example, as summarized by [3], bridge collapses due to liquefaction have been observed during the 1964 Niigata (Japan) and Alaska earthquakes, 1975 Haicheng (China) earthquake, 1976 Tanshang (China) earthquake, 2008 Wenchuan (China) earthquake and 2010 Maule (Chile) earthquake. Hence, understanding the initiation mechanisms of static and dynamic liquefaction (induced by cyclic loading) is very important for geotechnical engineers to predict and manage these associated hazards.

The undrained triaxial compression tests, triaxial extension tests and simple shear tests have been frequently conducted to examine the undrained soil behavior under a static loading (e.g., [1, 4-9]). Fig. 1 presents typical responses during the undrained triaxial compression tests carried out by [10]. For a loose sample with a void ratio of 0.93, the deviatoric stress $q = \sigma_v' - \sigma_r'$ initially increases with increasing shear strain (γ) until the soil reaches the peak state (as shown by the solid triangle in Fig. 1a), and the mean effective stress $p' = (\sigma_v' + 2\sigma_r')/3$ decreases with increasing γ. Note that σ_v' and σ_r' are the vertical and radial effective stresses, respectively. The shear strain γ is described by $\gamma = \varepsilon_a - \varepsilon_r$, where ε_a and ε_r are the vertical and radial strains, respectively. After the peak state, both the values of p' and q decrease with increasing γ until liquefaction ($p' = q = 0$). For the dense sample with a void ratio of 0.861, the deviatoric stress q continuously increases with increasing γ, and p' initially decreases and then increases with increaseing γ. In addition, for the medium dense sand with a void ratio of 0.868, q initially increases and then decreases with increasing γ, which is similar to the response in the early stage of undrained compression for a loose sample. Afterwards, the sample reaches a quasi-steady state (as shown by the solid circle in Fig. 1a), and then both the values of p' and

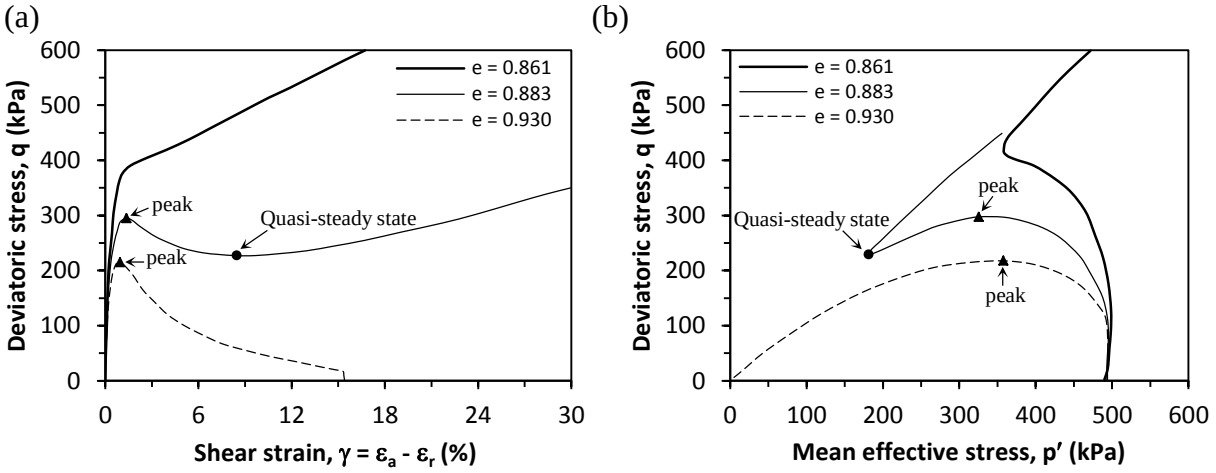

Figure 1: Typical responses during the undrained static compression tests: (a) stress-strain responses and (b) stress paths (after [10]).

q increase with increasing γ, which is similar to the response in the latter stage of a dense sample. Hence, the liquefaction state cannot be reached for the medium dense to dense samples. This explains why most of the case histories of static liquefaction occur in very loose to loose sand but not in medium dense to dense sand. However, the micromechanical basis of static liquefaction cannot be obtained based on these experimental observations.

To understand the undrained soil behavior under a cyclic loading, cyclic undrained simple shear tests and cyclic undrained triaxial tests have been carried out (e.g., [11-17]). Fig. 2 presents typical responses of a dense sample during a cyclic undrained triaxial test conducted by [18]. After isotropic consolidation, the sample was subjected to a cyclic loading under a stress-controlled undrained condition. The initial liquefaction seems to be reached at the 9th cycle, and the butterfly shaped loops have been reached afterwards (as shown in Fig. 2b). As noted, the values of the double amplitude axial strain (DA) for the cycles after initial liquefaction are much larger than those before initial liquefaction. Those experimental responses explain why liquefaction can occur in medium dense to dense sand during earthquakes. However, once again, the associated initiation mechanisms from a micromechanical perspective cannot be provided by these experiments.

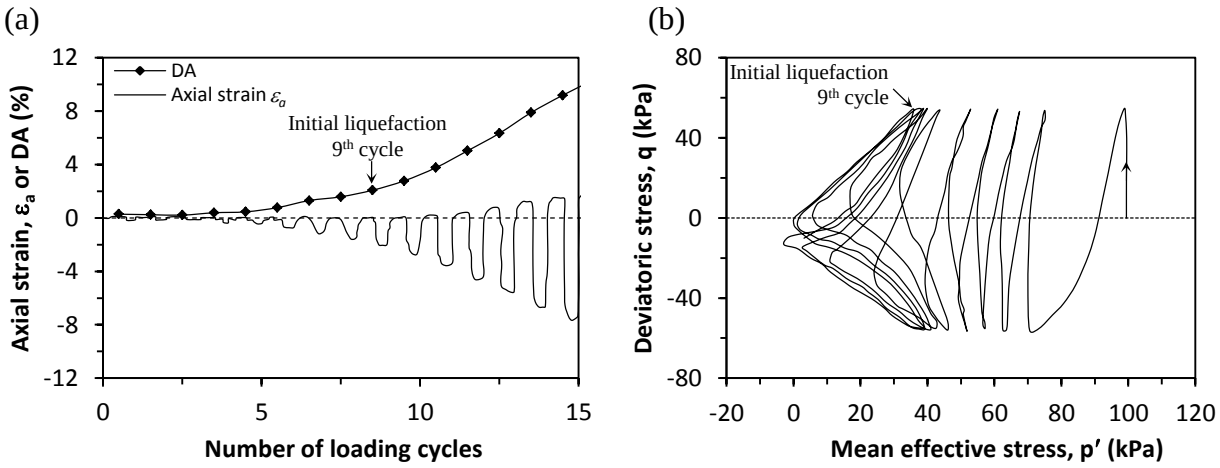

Figure 2: Typical responses during a cyclic undrained triaxial test (after [18]): (a) variations of the axial strain ε_a and double amplitude axial strain (DA) with the number of cycles and (b) stress paths. Note that only the stress paths for the initial nine loading cycles are shown in Fig. 2b. The stress paths for the following cycles are similar to the stress path for the 9th cycle.

Numerical simulations using the discrete element method (DEM) have been used to simulate the undrained soil responses for further analyses and examinations (e.g, [19-27]). Using DEM simulations can obtain not only the macroscopic stress and strain responses but also the information at the particle and contact scales, e.g., contact forces. Hence, DEM simulations can be used to effectively elucidate the involved micromechanical. Soroush & Ferdowsi [21] carried out DEM simulations of strain-controlled cyclic loading tests and qualitatively analyzed the variations of the contact force distribution with increasing number of loading cycles. However, quantitative and statistical analyses for the cyclic loading processes, especially for the stress-controlled cyclic loading, remain insufficient.

The objective of this study is to examine the initiation mechanisms of static liquefaction and dynamic liquefaction (induced by cyclic loading) from the micromechanical perspective. A series of DEM simulations of undrained triaxial compression tests and a cyclic undrained triaxial test are carried out. The simulations first aim to reproduce experimental findings (as

shown in Figs. 1 and 2). Then, variations of the contact force distributions are examined to explore the initiation mechanisms of liquefaction.

2 DETAILS OF THE DEM SIMULATIONS

The DEM software, Particle Flow Code in 3 Dimensions (PFC3D version 4.0, Itasca Company, USA) was used in this study. The Hertz-Mindlin contact model was used to regulate the force-displacement relationships in the normal and tangential directions. In addition, a rolling resistance model was adopted to account for the contact moments including the interlocking effects between real soil particles. Details of these contact models and the calibration of the parameters can be found in [28]. Table 1 summarizes the values of the parameters used in the DEM simulations.

Sample properties and parameters	Value
Contact model parameters	
Shear modulus G	1.0 GPa
Poisson's ratio ν	0.2
Inter-particle friction coefficient μ	0.32
Rolling stiffness coefficient J_n	2
Maximum rolling resistance coefficient μ_r	12
Particle size	
Largest particle diameter	0.212 mm
Smallest particle diameter	0.150 mm
Mean particle diameter d_{50}	0.172 mm
Properties of the samples	
Particle number	13528
Void ratio of the samples for UC1 and UC1-cyclic	0.745
Void ratio of the sample for UC2	0.783
Void ratio of the sample for UC3	0.792
Local damping used to dissipate kinetic energy	0.7

Table 1: Sample properties and parameters used in the DEM simulations of this study

Three DEM simulations of undrained triaxial compression tests were conducted. These simulations are denoted by UC1, UC2 and UC3 in the following discussion. The radius expansion method was used to prepare the samples. Particles were firstly generated with radii smaller than the assigned values and randomly positioned in the sample container, and then these radii were expanded to achieve the assigned values by multiplying a factor. After that, particles were rearranged under a friction-free condition where the inter-particle friction coefficient μ is set to be 0. When the sample reached equilibrium, the values of μ were set as 0.12, 0.18 and 0.20 for the samples of UC1, UC2 and UC3, respectively. The samples were then compressed under a confining pressure of 20 kPa. After this stage, the value of μ was increased to the assigned value, i.e., 0.32, for each sample, followed by an isotropic compression until the stress reached 100 kPa. As illustrated in Table 1, the void ratios were 0.745, 0.783 and 0.792 for the samples of UC1, UC2 and UC3, respectively before shearing. The samples were subjected to a strain-controlled undrained compression for shearing. Note that the undrained condition was simulated by applying boundary movements on the sample to make the sample volume maintain constant, which follows the same as the general practice.

In addition to those simulations of undrained compression tests, a simulation of a cyclic undrained triaxial test was conducted. The sample was identical to that used in UC1 after isotropic consolidation under a confining pressure of 100 kPa, and then the sample was subjected to a stress-controlled cyclic loading with the maximum deviatoric stress of 60 kPa. Note that both the values of the confining pressure after isotropic compression and the maximum deviatoric stress during cyclic loading were the same as those used in the experiment shown in Fig. 2. This test is denoted as UC1-cyclic in the following discussion.

3 SIMULATION RESULTS

3.1 Undrained compression tests

Fig. 3 presents the simulation results of the undrained compression tests, UC1, UC2 and UC3. Similar responses like the experimental findings (as shown in Fig. 1) are reproduced by the DEM simulations. To obtain the associated mechanisms from a micromechanical perspective, variations of the contact force distribution in terms of the mean and the coefficient of variation (COV) are examined in the following discussion.

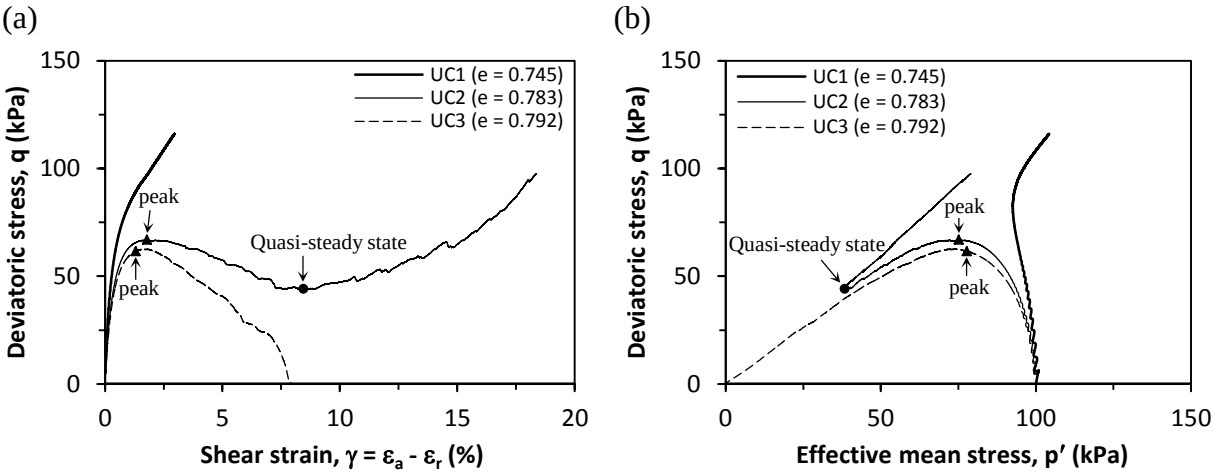

Figure 3: Simulation results of the undrained compression tests UC1, UC2 and UC3: (a) stress-strain responses and (b) stress paths.

Figs. 4a and 4b present variations of the mean and the COV of contact normal forces during the undrained compression tests, respectively. Fig. 7 presents the evolution of the mean value versus COV. Note that Fig. 7 summarizes the results from all the simulation cases and show that there are different trends of the mean versus COV for the samples with different void ratios. For loose sample UC3, the mean of contact forces decreases with increasing shear strain γ, while the associated COV increases with increasing γ. An interesting point is that these trends occur during both stages, i.e., before and after the peak state. This suggests that these trends, i.e., a decrease in the mean and an increase in the COV, are not influenced by the change of the deviatoric stress q with increasing γ.

For the medium dense sample UC2, the variations of the mean value and COV before the quasi-steady state are similar to those for UC1. Those trends of decreasing the mean value and increasing COV are also observed before the peak state and from the peak state to the quasi-steady state. However, after the steady state, the mean of contact normal forces increases with increasing γ, while COV decreases with increasing γ. This demonstrates that the contact nor-

mal forces become more and more uniform after the quasi-steady state. For the dense sample UC1, the initial responses are also showing a decrease in the mean and an increase in COV. However, the evolution trend of contact force distributions is different in the subsequent compression stage, which is found increasing in both the mean and the COV. Hence, the evolution type of the contact force distributions might be considered as the micromechanical basis for static liquefaction in loose sand.

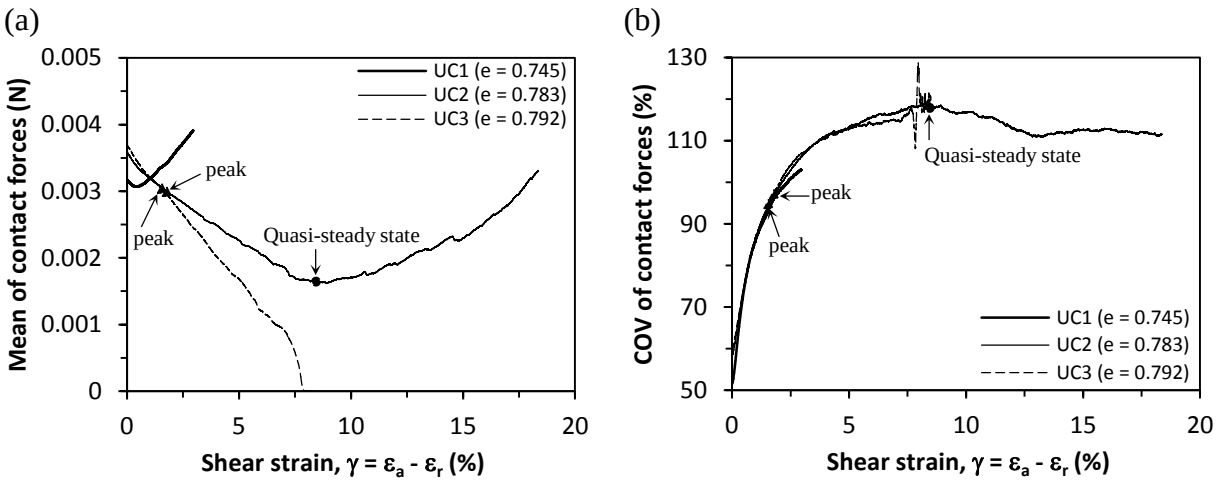

Figure 4: Variations of (a) the mean of contact normal forces and (b) the COV of contact normal forces during the undrained compression tests.

3.2 Cyclic undrained triaxial test

Fig. 5 presents the simulation results of the cyclic undrained triaxial test, UC1-cyclic. Once again, similar responses like the experimental findings (as shown in Fig. 2) are reproduced by the DEM simulations. Fig. 5b demonstrates that the soil reached the initial liquefaction state ($p' = q = 0$) at the 9th cycle. As shown in Fig. 5a, the values of the double amplitude axial strain (DA) for the cycles after the initial liquefaction, i.e., the 9th and 10th cycles, are much larger than the values of DA for the cycles before the initial liquefaction, i.e., from the 1st to

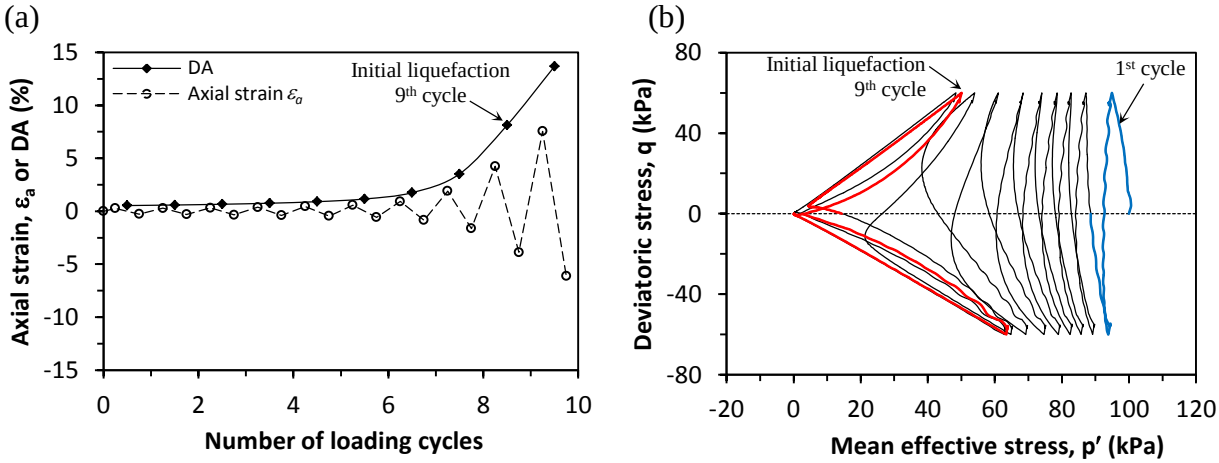

Figure 5: Simulation results of the cyclic undrained triaxial test UC1-cyclic: (a) variations of the axial strain ε_a and the double amplitude axial strain (DA) with the number of loading cycles and (b) stress paths. Note that only the minimum and maximum axial strains in a cycle are presented in Fig. 5a.

8th cycle. In the following discussion, variations of the mean and COV of all the contact normal forces are examined.

Figs. 6a and 6b present the variations of the mean and the COV of contact normal forces during the cyclic undrained triaxial test UC1-cyclic, respectively. For those loading cycles before initial liquefaction, there is a net decrease in the mean of contact normal forces and a net increase in the COV in each cycle, e.g., the 1st cycle. Hence, the overall trend for both the mean and the COV values at a given deviatoric stress q, e.g., q = 60 kPa, decreases in the mean and increases in the COV of contact normal forces. To facilitate the comparison between these results with those of the undrained compression tests, the mean versus the COV response of the test UC1-cyclic is also included in Fig. 7. As shown in Fig. 7, the mean versus COV response during the initial loading stage in the 1st cycle is identical to that during UC1. However, the mean versus COV response in the subsequent unloading process in UC1-cyclic does not follow the original trend as in the loading process. The overall trend of the mean versus COV response is characterized by a decreased mean and increased COV of contact normal forces, which is similar to the behavior of undrained compression for a loose sample, i.e., UC3. This suggests that this evolution type of contact force distribution can also be used to explain the initiation mechanisms of the liquefaction induced by cyclic loading from a micromechanical perspective.

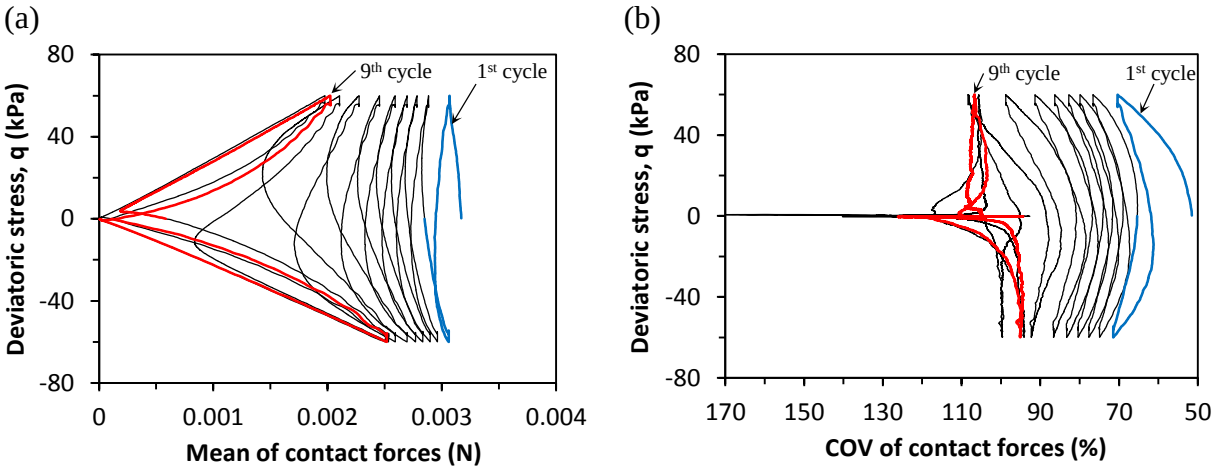

Figure 6: Variations of (a) the mean of contact normal forces and (b) the COV of contact normal forces during the cyclic undrained triaxial test.

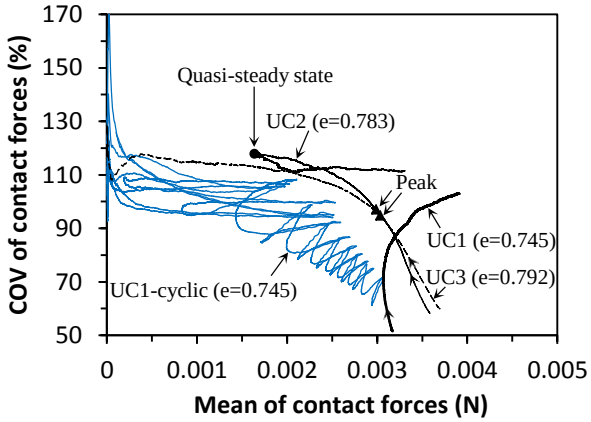

Figure 7: The mean versus the COV of contact forces responses for the undrained compression tests, i.e., UC1, UC2 and UC3, and the cyclic undrained triaxial test UC1-cyclic.

4 CONCLUSIONS

To examine the initiation mechanisms of static liquefaction and dynamic liquefaction induced by cyclic loading, a series of DEM simulations of undrained triaxial compression tests and a cyclic undrained triaxial test were carried out. The DEM simulation results can reproduce similar responses like the experimental findings, e.g., stress-strain responses and stress paths. Changes in the contact force distribution were examined in terms of mean and COV of contact normal forces. The salient findings are summarized as follows.

The mean versus COV response during undrained compression tests is influenced by the sample void ratio. For the loose sample, the evolution type is characterized by a continuous decrease in the mean value and a continuous increase in the COV as the shear strain increases. For the medium dense sample, the response before the quasi-steady state is similar to that observed in the loose sample, whereas the response after the quasi-steady state demonstrates an increase in the mean and a decrease in the COV. In addition, for the dense sample, the mean value initially decreases and then increases with increasing shear strain while the COV continuously increases with increasing shear strain. Hence, the evolution type characterized by a continuous decrease in the mean value and a continuous increase in the COV might be considered as the micromechanical basis for static liquefaction in loose sand. In fact, such an evolution type of mean versus COV can also be found in the DEM simulation of cyclic undrained triaxial test on a dense sample. That is, this evolution type of contact force distribution, i.e., a decrease in mean and an increase in COV, can serve as a basis to explain the initiation mechanisms of static and dynamic liquefaction from a micromechanical perspective.

ACKNOWLEDGEMENT

This research was supported by the Hong Kong Research Grants Council (HKUST9/CRF/09 and HKUST6/CRF/12R). The authors are grateful to the reviewers for their valuable comments.

REFERENCES

[1] J.A. Yamamuro, P.V. Lade, Static liquefaction of very loose sands. *Canadian Geotechnical Journal*, **34**, No. 6, 905-917, 1997.

[2] H.B. Seed, Soil liquefaction and cyclic mobility evaluation for level ground during earthquakes. *Journal of the Geotechnical Engineering Division*, **105**, No. 2, 201-255, 1979.

[3] S. Bhattacharya, A. Kappos, On the collapse of bridge foundations in liquefiable soils during earthquakes. In *2ed European Conference on Earthquake Engineering and Seismology*, Istanbul, August 25-29, 2014.

[4] K. Ishihara, Liquefaction and flow failure during earthquakes. *Géotechnique*, **43**, No. 3, 351-451, 1993.

[5] P.V. Lade, Creep effects on static and cyclic instability of granular soils. *Journal of Geotechnical Engineering*, **120**, No. 2, 404-419, 1994.

[6] T. Doanh, E. Ibraim, R. Matiotti, Undrained instability of very loose Hostun sand in triaxial compression and extension. Part 1: experimental observations. *Mechanics of Cohesive‐frictional Materials*, **2**, No. 1, 47-70, 1997.

[7] M. Yoshimine, K. Ishihara, Flow potential of sand during liquefaction. *Soils and Foundations*, **38**, No. 3, 189-198, 1998.

[8] M. Yoshimine, P.K. Robertson, C.E. Wride, Undrained shear strength of clean sands to trigger flow liquefaction. *Canadian Geotechnical Journal*, **36**, No. 5, 891-906, 1999.

[9] E. Ibraim, H. Di Benedetto, T. Doanh, Time-dependent behaviour and static liquefaction phenomenon of sand. *Geotechnical and Geological Engineering*, **27**, No. 1, 181-191, 2009.

[10] R. Verdugo, Characterization of sandy soil behavior under large deformation. Ph.D. thesis, University of Tokyo, 1992.

[11] K. Ishihara, H. Takatsu, Effects of overconsolidation and K_0 conditions on the liquefaction characteristics of sands. *Soils and Foundations*, **19**, No. 4, 59-68, 1979.

[12] Y. Yoshimi, K. Tokimatsu, Y. Hosaka, Evaluation of liquefaction resistance of clean sands based on high-quality undisturbed samples. *Soils and Foundations*, **29**, No. 1, 93-104, 1989.

[13] M.D. Evans, S. Zhou, Liquefaction behavior of sand-gravel composites. *Journal of Geotechnical Engineering*, **121**, No. 3, 287-298, 1995.

[14] D. Erten, M.H. Maher, Cyclic undrained behavior of silty sand. *Soil Dynamics and Earthquake Engineering*, **14**, No. 2, 115-123, 1995.

[15] T. Kokusho, T., Hara, R. Hiraoka, Undrained shear strength of granular soils with different particle gradations. *Journal of Geotechnical and Geoenvironmental Engineering*, **130**, No. 6, 621-629, 2004.

[16] V.N. Ghionna, D. Porcino, Liquefaction resistance of undisturbed and reconstituted samples of a natural coarse sand from undrained cyclic triaxial tests. *Journal of geotechnical and geoenvironmental engineering*, **132**, No. 2, 194-202, 2006.

[17] M.L. Taylor, M. Cubrinovski, B.A. Bradley, Cyclic strength of Christchurch sands with undisturbed samples. *New Zealand Society for Earthquake Engineering Annual Conference (NZSEE2013)*, Wellington, New Zealand, April 26-28, 2013.

[18] H.Y. Sze, J. Yang, Failure modes of sand in undrained cyclic loading: impact of sample preparation. *Journal of Geotechnical and Geoenvironmental Engineering*, **140**, No. 1, 152-169, 2013.

[19] T.T. Ng, R. Dobry, Numerical simulations of monotonic and cyclic loading of granular soil. *Journal of Geotechnical Engineering*, **120**, No. 2, 388-403, 1994.

[20] X. Li, Micro-scale investigation on the quasi-static behavior of granular material. 2006. Ph.D. thesis, Hong Kong University of Science and Technology.

[21] A. Soroush, B. Ferdowsi, Three dimensional discrete element modeling of granular media under cyclic constant volume loading: a micromechanical perspective. *Powder Technology*, **212**, No. 1, 1-16, 2011.

[22] G. Gong, P. Lin, Y. Qin, J. Wei, DEM simulation of liquefaction for granular media under undrained axisymmetric compression and plane strain conditions. *Acta Mechanica Solida Sinica*, **25**, No. 6, 562-570, 2012.

[23] G. Gong, X. Zha, C. Wan, A microscopic definition of liquefaction for sand. *Procedia Earth and Planetary Science*, **5**, 140-145. 2012.

[24] A. Dabeet, D. Wijewickreme, P. Byrne, Simulation of cyclic direct simple shear loading response of soils using discrete element modeling. In *15th World Conf. Earthquakes Eng.* Lisboa, 2012.

[25] M.R. Kuhn, H.E. Renken, A.D. Mixsell, S.L. Kramer, Investigation of Cyclic Liquefaction with Discrete Element Simulations. *Journal of Geotechnical and Geoenvironmental Engineering*, **140**, No. 12, 2014.

[26] A. Dabeet, D. Wijewickreme, P. Byrne, Application of discrete element modeling for simulation of cyclic direct simple shear response of granular materials. In *National Conference on Earthquake Engineering*, Anchorage, Alaska, July 21-25, 2014.

[27] J. Wei, G. Wang, Cyclic mobility and post-liquefaction behaviors of granular soils under cyclic loading: micromechanical perspectives. In *10th U.S. National Conference on Earthquake Engineering*, Anchorage, Alaska, July 21-25, 2014.

[28] Z. Zhang, Y.H. Wang, Three-dimensional DEM simulations on monotonic jacking in sand. Submitted to *Granular Matter*, 2015.